REVIEWS SCIENCE CHINA Materials

mater.scichina.com link.springer.com

Published online 20 April 2015 | doi: 10.1007/s40843-015-0047-0
Sci China Mater 2015, 58: 302–312

Tunable magnetic and electrical behaviors in perovskite oxides by oxygen octahedral tilting

Ya Gao[1], Jianjun Wang[1,2], Liang Wu[1], Shanyong Bao[1], Yang Shen[1], Yuanhua Lin[1*] and Cewen Nan[1*]

The oxides with perovskite structure possess abundant physical properties, such as magnetism, dielectricity, photoelectricity, ferroelectricity, etc. The oxygen ions in the perovskite unit cell constitute an octahedral distribution. The deformation or tilting of the special oxygen octahedra structure leads to new performances or properties change. Here, we give a review of the relationship between magnetic and electrical behaviors and oxygen octahedral tilting in several typical perovskite oxides. An understanding of how to tune these properties by controlling the tilting during the sample growth can more effectively guide the design of new structures for high performance and inspiring their potential applications.

INTRODUCTION

The ABO_3 type oxides have the atoms arranged into the so-called perovskite structure. One perovskite unit cell involves six oxygen atoms, which occupy the face-centered sites of the face-centered cubic (FCC) structure, forming an oxygen octahedron, and the B-site cations infill the central vacancy, as shown in Fig. 1a. In a centrosymmetrical perovskite such as $SrTiO_3$ [1–3] with space group of *Pm*3*m* and lattice parameter of 3.905 Å, the strontium ions are located at the corners of the cubic unit cell, and the titanium ion is in the center, surrounding by oxygen ions. These TiO_6 octahedra are perfectly piled up in three dimensions, with 90° angles and six equal Ti–O bonds at a length of 1.952 Å, as shown in Fig. 1b. For the non-ideal cases, the atom arrangement has diverse possible distortions, including: 1) deformation of the oxygen octahedra arising from Jahn-Teller effect, which changes the cubic symmetry and results in metal-insulator transitions in some oxides, or the arrangement of the spin in B-site atoms and then the change of magnetic properties [4]; 2) displacement of the center cation inside the oxygen octahedra giving rise to ferroelectricity, which is the situation of $BaTiO_3$ [5,6] and $Pb(Zr_{1-x}Ti_x)O_3$ [7]; 3) in a wide range, oxygen octahedral tilting or rotation which can define the symmetry of the material [8]. One of the structural distortions or the combination among them (Fig. 1c) can form a unique perovskite structure [9]. The structural distortions are related to diverse functionalities such as ferroelectricity [10–12], dielectricity [13,14], electroconductivity [15], thermal conductivity [16], superconductivity [17], catalysis oxidation [18], photoelectricity [19], magnetism [20,21], and multiferroicity [22,23].

As early as 1972, Glazer [8,24] defined the classification of the oxygen octahedral tilting in perovskites, which was called the Glazer notation: $\mathbf{a^l b^m c^n}$, where a, b and c repre-

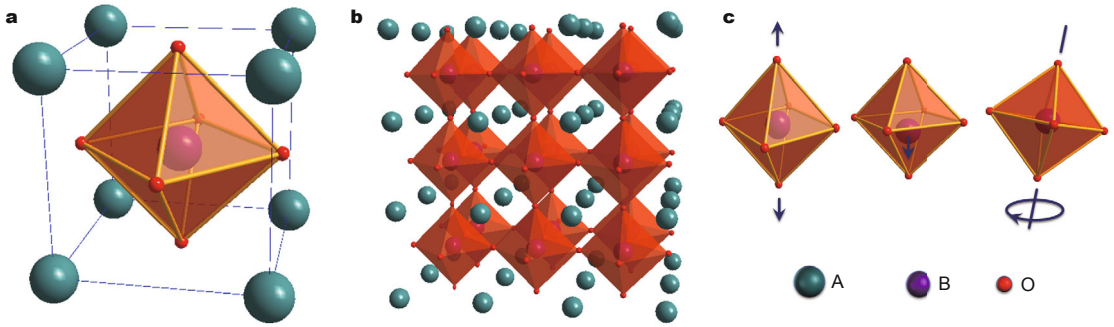

Figure 1 (a) Schematic of an ABO_3 perovskite unit cell and its oxygen octahedron (orange). (b) Ideally arranged unit cell and octahedral configuration. (c) Possible distortions for non-ideal structures: Jahn-Teller elongation, center cation displacement, and oxygen octahedral tilting. Reproduced with permission from Ref. [9] (Copyright 2010, American Physical Society).

[1] School of Materials Science and Engineering, and State Key Laboratory of New Ceramics and Fine Processing, Tsinghua University, Beijing 100084, China
[2] Department of Materials Science and Engineering, Pennsylvania State University, University Park, Pennsylvania 16802, USA
* Corresponding authors (emails: linyh@mail.tsinghua.edu.cn (Lin Y); cwnan@mail.tsinghua.edu.cn (Nan C))

sent the tilting magnitudes around the [100], [010] and [001] axes of the cubic or pseudo-cubic unit cell, while the superscripts ***l***, ***m***, and ***n*** are +, − or 0, expressing the tilting angle of the neighbor octahedron tilts in the same (+,"in-phase" type) or opposite (−, "anti-phase type") sense, or no tilts (0). The origin of the oxygen octahedron tilting is reflected by the deviation of the B–O–B bond which can be described by two quantitative definitions. The first is Goldschmidt Tolerance Factor [25]:

$$t = \frac{r_A + r_O}{\sqrt{2}(r_B + r_O)}, \quad (1)$$

where r_A, r_B and r_O are radii of A, B cations and O anions, respectively. The second is the Intersection Angle of the two bonds:

$$\theta = \langle \text{B–O–B} \rangle. \quad (2)$$

For a centrosymmetrical perovskite wherein the A cation matches in size with the O anion to form cubic close-packed layers and the B cation matches the size of the interstitial sites of the BO_6 octahedron, the tolerance factor (t) is 1. However, once a distortion happens, the ideal packing will be broken, and t will deviates from 1.0 with the deviation reflecting how far the ionic sizes can move and still be "tolerated" by the perovskite structure. When the deviation of t from 1.0 is small, e.g., $-0.05 \leqslant t-1.0 \leqslant 0.04$, the crystal structures were found to preserve cubic symmetry [26,27]. Whereas, if the deviation is positive and relatively large, for example in $Ba_5Ta_4O_5$ [28], the B–O bonds are tensed while A–O bonds are compressed, and the B–O–B bond angle θ remains 180°, leading to hexagonal atomic stacking accompanied by ferroic properties. Likewise, if the deviation is negative and relatively large, the A–O bonds are tensed while the B–O bonds are compressed, resulting in the tilting of the oxygen octahedra and the bent of the B–O–B bonds. Such distortion gives rise to tetragonal stacking (rotate around [001] axis, *I*4/*mcm* or *P*4/*mbm* systems), rhombohedral stacking (rotate around [111] axis, $R\bar{3}c$ or $Im\bar{3}$ systems), or orthorhombic stacking (rotate around [110] or [001] axis, *Pbnm* or *Pnma*) [29], and the average bond angle θ continues to decrease as the symmetry change from tetragonal to rhombohedral to orthorhombic. Therefore the tolerance factor and the oxygen octahedral tilting are criteria for the structure symmetry.

The tilting of oxygen octahedra is highly related to the tunable properties of the perovskite oxides. In this review, we use four prototypes as examples to present the relationship between the oxygen octahedral tilting and the magnetic and electric properties of the perovskite ABO_3 oxides.

MAJOR TECHNIQUES TO OBSERVE OXYGEN OCTAHEDRAL TILTING

The magnitude of the oxygen octahedron tilting can be evaluated from both theoretical calculations and experiments. Theoretically, calculation methods [30–32] can work from atom arrangements and predict the connection between the oxygen octahedral tilting and the properties. Fig. 2a gives an example of a complete new family of stable phases in multiferroic $BiFeO_3$ (BFO) and related compounds [33]. Besides the $\mathbf{a^0a^0c^+}$ (*c* axis in-phase type, namely *pp* or *mm*) and $\mathbf{a^0a^0c^-}$ (*c* axis anti-phase type, namely *pm*) tilting patterns, it is also possible that the BFO displaces complex and nano-twinned tilting patterns, *ppmppm* and *ppmm*.

Experimentally, researchers first started with neutron deflections measurements [34–36] to characterize the structure symmetry. With the development of electron microscope, experimental observations can directly spot

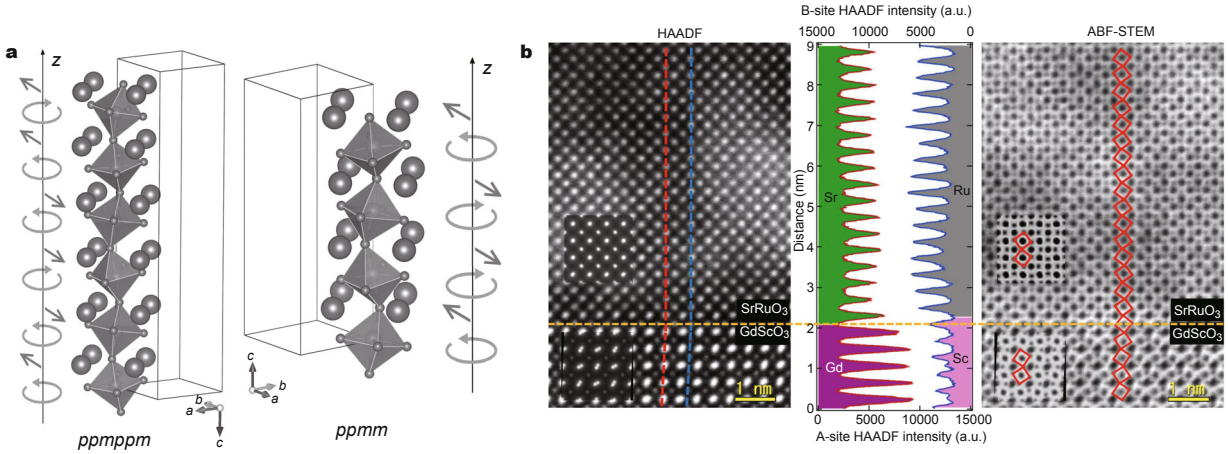

Figure 2 Methods to characterize the oxygen octahedral tilting. (a) Calculation prediction of possible tilting superstructure in BFO (Reprinted with permission from Ref. [33], Copyright 2012, John Wiley and Sons). (b) Direct observation through HAADF and ABF-STEM of the tilting at SRO/GSO interface (Reprinted with permission from Ref. [37], Copyright 2013, Nature Publishing Group).

the octahedra. For example, with the help of the high-angle annular dark field scanning transmission electron microscopy images (HAADF-STEM) and annular bright-field scanning transmission electron microscopy (ABF-STEM), it is available to visualize the oxygen atoms as well as the octahedral tilting. Fig. 2b shows the oxygen octahedra of a $SrRuO_3$ (SRO) film on the $GdScO_3$ (GSO) substrate [37], where the tilting is $\mathbf{a}^-\mathbf{a}^-\mathbf{c}^+$ in an orthorhombic (*Pbmn*) structure, and the pattern of the film gradually changes from in-plane along $[001]_{ortho}$ to out-of-plane along $[1–10]_{ottho}$. Also, Ramen spectrum can help to measure the structural distortion [38–40].

OXYGEN OCTAHEDRAL TILTING TUNNING MAGNETIC BEHAVIOR

Multiferroic $BiFeO_3$ (BFO)

BFO is the only material that has been discovered to maintain both magnetism and strong ferroelectricity at room-temperature, with antiferromagnetic Néel temperature T_N~643 K, and ferroelectric Curie temperature T_C~1103 K [41,42]. Fig. 3a shows the schematic illustration of a BFO unit cell, which is rhombohedrally (*R*) distorted (*R*3*c*) [43] with lattice parameters of a = 3.965 Å and α = 89.3°–89.4° [44,45], meanwhile, the tolerance factor t = 0.88 [46], and the Fe–O–Fe angle θ = 154°–156° [47]. The oxygen octahedral tilting is about 11°–14° around the [111] axis [43,48] (Glazer notation $\mathbf{a}^-\mathbf{a}^-\mathbf{a}^-$). Such tilting controls both the magnetic exchange and the orbital overlap between Fe and O ions, thus determines the magnetic ordering temperature and the conductivity (which will be discussed in the later section).

The local short-range magnetic ordering of BFO is G-type antiferromagnetism, with each Fe^{3+} spin surrounded by the six antiparallel spins on the nearest Fe neighbors. Yet, the spins are not perfectly antiparallel due to the oxygen octahedral tilting, and this asymmetry is intimately connected with a macroscopic magnetization called weak ferromagnetism [49], arising from the canting of the antiferromagnetic sublattices. However, there is a spiral spin structure (a spin cycloid, Fig. 3b) with the antiferromagnetic axis rotating along the [10-1] direction in a long-wavelength period of 64 nm [50], which cancels the local canted moment as an averaging out effect in bulk BFO. Fortunately, this spin cycloid can be suppressed by doping [51] or in thin films due to epitaxial constraints from the substrates or enhanced anisotropy [52], which enables a homogeneous net magnetic moment. The mechanism of the canted moment is an antisymmetric spin coupling called Dzyaloshinskii-Moriya (DM) interaction [53,54], which is due to the combined action of exchange interaction and spin-orbit coupling. Between two magnetic moments $\mathbf{M}_{Fe1}$ and $\mathbf{M}_{Fe2}$ of two Fe atoms in the unit cell, as shown in Fig. 3c, DM interaction has the form of:

$$E_{DM} = -\frac{1}{2}\mathbf{D}\cdot(\mathbf{M}_{Fe1}\times\mathbf{M}_{Fe2}) = -\mathbf{D}\cdot(\mathbf{L}\times\mathbf{M}_c), \qquad (3)$$

where $\mathbf{D}$ is the coupling vector, $\mathbf{L} = \mathbf{M}_{Fe1} - \mathbf{M}_{Fe2}$ is the an-

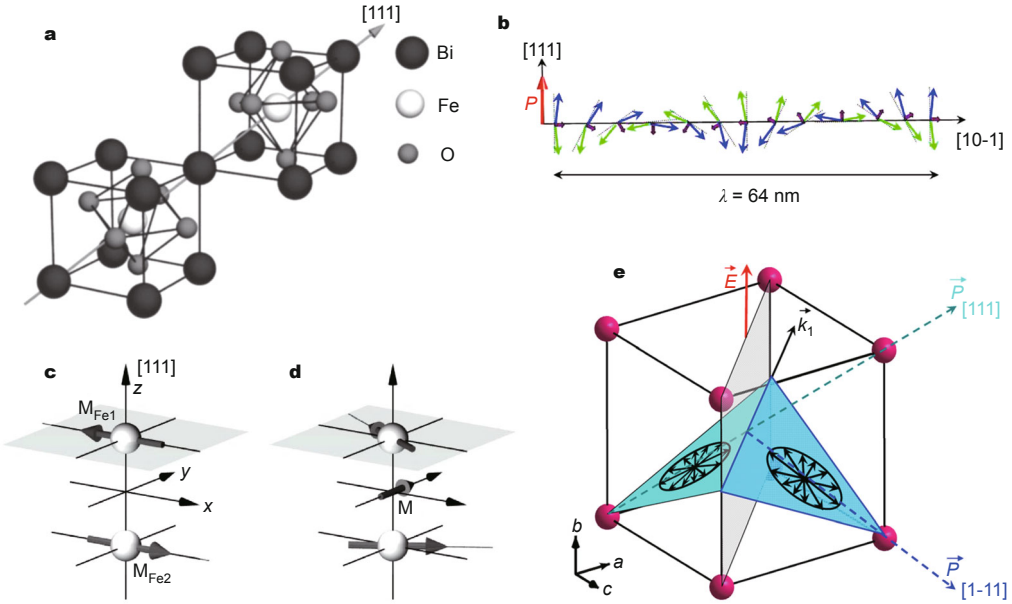

Figure 3 (a) Schematic of the *R*3*c* BFO unit cell. (b) Schematic of the spin cycloid in bulk BFO. (c and d) Schematic of the magnetic moment arrangement of two Fe ions in BFO, from antiferromagnetically oriented (c) to spin-orbit interaction induced canted configration (d). (e) Relationship between the magnetic easy plane and the ferroelectric polarization. Reprinted with permission from Ref. [49] and [50] (Copyright 2005 and 2008, American Physical Society).

tiferromagnetic vector which express the difference of the two sublattice magnetizations, and $\mathbf{M}_c = \mathbf{M}_{Fe1} + \mathbf{M}_{Fe2}$ is the resulting canted magnetization (Fig. 3d). From the expression of E_{DM}, it is clear that **D, L** and **M** build up a right-handed system. This DM interaction-induced weak magnetism has been proved by calculations [49] to be coupled with the structural distortions. On the other hand, besides the oxygen octahedral tilting, the structural distortions in *R*3*c* BFO also includes the anion and cation displacement which leads to a spontaneous electric polarization of about 100 μC cm^{-2} [55]. However, the experimentally observed magnetization reversal was demonstrated to link directly with the oxygen octahedral tilting instead of the polarization displacement switching.

Since BFO is also a rhombohedral ferroelectric, its polarization ***P*** points along [111] directions. Experimental works have explored the relationship between the ferroelectric polarization and the magnetic symmetry. The magnetic easy plane is defined by the polarization ***P*** and the cycloid propagation vector $\boldsymbol{k}//[10\bar{1}]$ in bulk BFO. Thus the homogeneous canted moment in thin films is perpendicular to the polarization, and can be manipulated by electrically switching the polarization, as shown in Fig. 3e. Recently, it is reported both theoretically and experimentally that in an exchange coupled $Co_{0.9}Fe_{0.1}$ (CoFe)/BFO heterostructure, the ferromagnetic moment of CoFe can be reversed using applied electric field, which is promising candidate for magnetoelectric and multiferroic device applications [56,57].

By manipulating the epitaxial strain to be strongly compressive in BFO thin films (using $YAlO_3$ and $LaAlO_3$ substrates instead of $SrTiO_3$ or $DySrO_3$), the rhombohedrally symmetry in bulk BFO can be manipulated to a tetragonal-like (*T*-phase) distorted phase (*P*4*mm*), with the lattice parameter *a*~3.66 Å and *c*~4.65 Å [58]. Such distortion has a large spontaneous polarization, however it suppresses the oxygen octahedral tilting in *R*-phase BFO. Therefore, the *T*-phase BFO has been proved with no canted moment [59]. This is further evidence that the weak ferromagnetism is related to the tilting distortion instead of the ferroelectric B-site cation displacement. The $LaAlO_3$ substrates also produce appropriate compressive strain that the *T*- and *R*-phase coexist (mixed phase) in the films, which provide comprehensive yet interesting system for further studies.

Metallic ferromagnet (La,Ca)MnO_3 (LCMO) and (La,Sr)MnO_3 (LSMO)

With appropriate doping of Sr or Ca on the A-site, $LaMnO_3$ can be transformed from an antiferromagnetic insulator to a ferromagnetic metal, which is explained by the double exchange hoping mechanism [60–63] associated with Jahn-Teller effect [64]. Unlike BFO, LSMO [65] and LCMO [66] have multiple phase transitions: the rhombohedral-orthorhombic-monoclinic structural phase transitions, the electronic transport metal-insulator transition, and the antiferromagnetic-ferromagnetic phase transition. The phase diagrams of LSMO and LCMO are shown in Figs 4a and b. Such a complex doping system enhances the variety of physical properties. The LSMO with doping concentration *x* between 0.2 and 0.4 has the highest Curie temperature ($T_C \approx$ 370 K in thin films) in the manganite family, as well as relatively high carrier density (10^{21}–10^{22} cm^{-3}) [66]. It also has a perovskite structure with rhombohedral distortion (Glazer notation: $\mathbf{a}^-\mathbf{a}^-\mathbf{a}^-$), the tilting angle is 7.8°, and the Mn–O–Mn angle θ is about 163° [67].

In ideal crystal stacking of LSMO or LCMO, the energy-level configuration of the five d orbitals of a manganese ion split into a t_{2g} triplet and an e_g doublet. Under the effect of Jahn-Teller distortions, the energy of the t_{2g} triplet and the e_g doublet further split into a complex spin-resolved band structure [68,69]. The spin-up localized t_{2g} band are fully occupied, thus the conductivity are determined by the partially occupied spin-up e_g band and the oxygen p bands. Moreover, the coexistence of Mn^{3+} and Mn^{4+} gives rise to absence electrons (or holes) of the Mn^{4+} e_g orbit, which can contribute to conductivity. In details, an O_{2p} electron hops to a Mn^{4+} empty e_g orbital, meanwhile, the e_g electrons of the adjacent Mn^{3+} hops to the O_{2p} orbital. With strong Hund's coupling, the spin of the e_g electron is parallel to the t_{2g} electrons in Mn^{3+} (Mn^{4+}). Such ferromagnetic interaction caused by the exchange of conduction electrons is called double exchange interaction. The hopping probability of the e_g electrons between adjacent *i* and *j* Mn ions along the Mn–O–Mn chain can be explained by the effective hopping energy t_{ij}:

$$t_{ij} = t_{ij}^0 \cos\frac{\theta_{ij}}{2}, \tag{4}$$

where t_{ij}^0 is the intersite hopping interaction, and θ_{ij} is the angle between the classic t_{2g} spins of the Mn ions. The equal sign establishes under certain hypothesis and approximation. According to Equation (4), the energy is largest when the Mn spins are aligned parallel. Therefore, by modifying the spin alignment, the conductivity can be manipulated. The spin configuration upon T_C is random, which leads to low hopping probability of the e_g electrons. However, an external magnetic field can align the spins, and results in magnetoresistance (MR) effect. Such enormous MR change around T_C is called colossal magnetoresistance (CMR) effect [68].

According to the mechanism of the CMR effect in LSMO or LCMO systems, Mn–O bond length and the Mn–O–Mn angle can control the hoping matrix elements and then affect the magnetism and transport properties. The

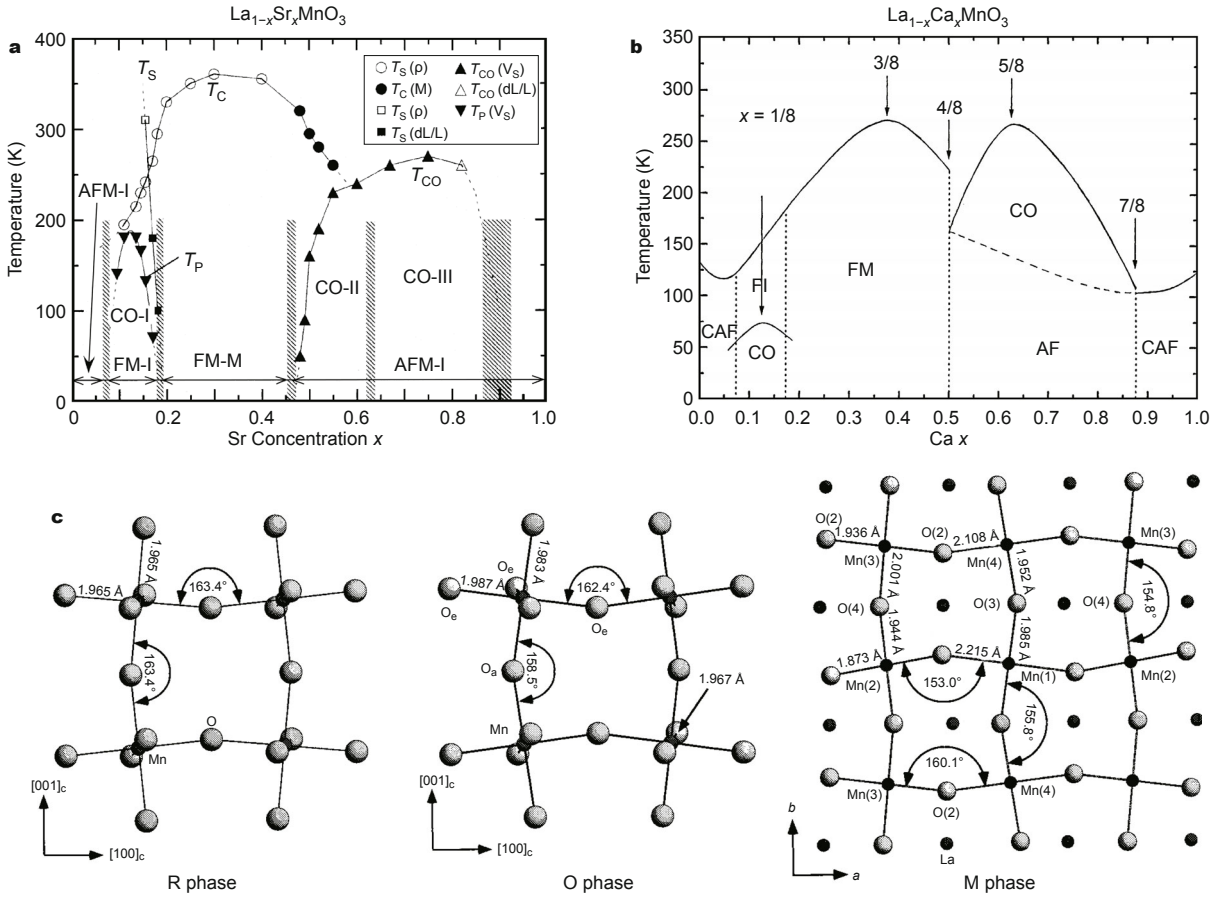

Figure 4 (a and b) Phase diagram of LSMO (a) (Reproduced with permission from Ref. [65], Copyright 1998, The Physical Society of Japan) and LCMO (b) (Reprinted with permission from Ref. [68], Copyright 2001, Elsevier). (c) Schematic of Mn–O bond length and the Mn–O–Mn bond angle in rhombohedral, orthorhombic and monoclinic phase LSMO, section view along the cubic (010) plane for R and O phase, and c axis for M phase (Reprinted with permission from Ref. [34], Copyright 1996, American Physical Society).

electron structures for rhombohedral ($R\bar{3}c$), orthorhombic ($Pbnm$), and monoclinic ($P2_1/c$) phases along (010) plane are shown in Fig. 4c [34]. It is reported that the monoclinic phase is antiferromagnetic, the rhombohedral phase is ferromagnetic, and the orthorhombic phase is ferromagnetic for $x \geqslant 0.125$. Transport measurements show that the orthorhombic and monoclinic samples remain nonmetallic from 20 to 350 K, while the rhombohedral phase exhibits a metal-insulator transition at temperatures close to T_C. By controlling the oxygen octahedral tilting in LSMO through epitaxial strain engineering, the novel structural, electronic, and magnetic behaviors can be designed in thin films and multilayers with desired properties [9].

OXYGEN OCTAHEDRAL TILTING TUNNING ELECTRICAL BEHAVIOR

Dielectricity: ABO_3 perovskite

The perovskite is the name for a particular mineral: $CaTiO_3$ (CTO) as well as being the name of a structural family. The CTO ceramic (a = 3.80 Å, t = 0.98, orthorhombic, tilting notation: $\mathbf{a^-a^-c^+}$) is a typical dielectric material (κ = 180 at room temperature) [70]. Thus the dielectric constant (ε_r) of the perovskite structure was the first useful property pursued in history. During the Second World War, $BaTiO_3$ (BTO) was spotted to be a promising material with highest ε_r [6,71,72]. The high dielectric susceptibility comes from the displacement of the titanium ions of the TiO_6 octahedra center, which also results in ferroelectricity. However, the tolerance factor of BTO at room temperature is above 1, indicating that there is no tilting required.

Afterwards, a series of barium and strontium based complex perovskites with the formula $A(B_{1/3}B'_{2/3})O_3$ were studied [4,73,74]. The B-site cations are stacked with one layer of B ions and two layers of B′ ions in the {111} planes, while the A-site cations gradual substitution of Sr for Ba reduces the t value and resulting in phase transitions including oxygen octahedral tilting. These doping induced

distortions affect the temperature coefficient of the dielectric permittivity (τ_ε) and resonant frequency (τ_f). Fig. 5a illustrates the relationship between the t value and τ_ε, which means that τ_ε is manipulated by the octahedral tilting related transitions. As the t value decreases from 1.06 to 0.92, the complex perovskites structure experienced from "untilted" to "anti-phase tilted" to "in phase and anti-phase tilted" modifications. The Glazer notations taken into consideration for the tilting modes are listed in Table 1. Because the compounds with higher temperature stability (τ_ε close to 0) and lower dielectric losses (high quality factor $Q{\cdot}f$) are more promising candidates for resonators, by changing the B-site cations and manipulating the Ba/Sr ratio, the tilting mode of the structure can be controlled, and the dielectric properties can be regulated.

Table 1 The possible Glazer notations for the oxygen octahedral tilting of Ba and Sr-based complex perovskites

Tilting mode	Possible Glazer notation
Untilted	$a^0a^0a^0$
Anti-phase tilted	$a^-a^-a^-$, $a^-b^-b^-$, $a^-b^-c^-$, $a^-a^-c^-$
In phase and anti-phase tilted	$a^+a^-a^-$, $a^+b^-b^-$, $a^+b^-c^-$, $a^+a^-c^-$

Dielectricity: complex perovskite (tungsten bronze structure)

Similarly, a perovskite-related solid solution $Ba_{6-3x}R_{8+2x}Ti_{18}O_{54}$ ($0 < x < 1$, where R is rare earth) also exhibits good dielectric properties as microwave resonators [75,76]. The structure is called tungsten bronze like superstructure (*Pbam*, *Pbnm*), in which the TiO_6 octahedra framework forming by 2 × 2 unit cells of perovskite blocks and producing ten A1 rhombic sites, four A2 pentagonal and four trigonal sites for A-site cations. The tolerance factor of this structure can be described by the following equation [77]:

$$t = \frac{\left[\left(\frac{4}{5}+\frac{x}{5}\right)r_{A1}+\left(\frac{1}{5}-\frac{x}{5}\right)r_{A2}\right]+r_O}{\sqrt{2}(r_B+r_O)}. \quad (4)$$

The tilting of oxygen octahedra (Fig. 5c) along the c ($[001]_{pseudo\text{-}cubic}$) axis leads to splitting of the oxygen ion electron density, which further changes the structure symmetry from *2* to 2_1 along the c axis, and then affects the dielectric properties.

It is reported [78] that the highest $Q{\cdot}f$ value of the $Ba_{6-3x}R_{8+2x}Ti_{18}O_{54}$ ceramic comes from the composition x = 2/3,

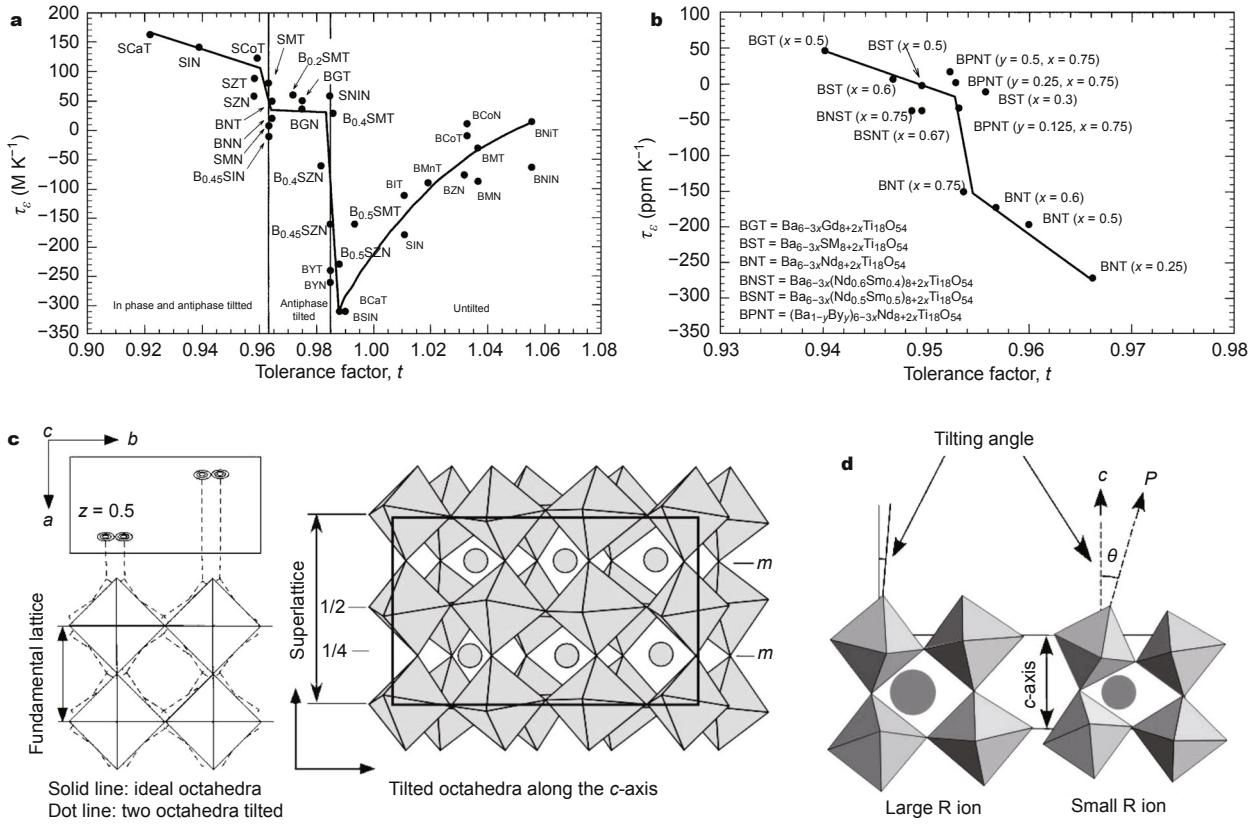

Figure 5 (a and b) Tolerance factor (t) *vs.* τ_ε for Ba and Sr-based complex perovskites (a) and tungsten bronze type compounds (b) (Reprinted with permission from Ref. [13], Copyright 2000, Springer). (c) Splitting of oxygen ion induced octahedral tilting in $Ba_{6-3x}R_{8+2x}Ti_{18}O_{54}$. (d) Dielectric constant ε_r concerned with tilting angle in $Ba_{6-3x}R_{8+2x}Ti_{18}O_{54}$ (Reprinted with permission from Ref. [80], Copyright 2001, Elsevier).

in which the barium ions and rare earth ions occupy the A2 and A1 sites, respectively. Such distribution of cation ordering reduces the internal strain of the structure and results in high *Q·f*. Nevertheless, the dielectric constant is affected by not only the volume of the TiO_6 octahedra, but also the tilting of the Ti–O–Ti bond, and the polarizabilities of the barium and the rare earth ions. For different R ions (Sm, Nd, Pr, and La), the ε_r decreases linearly as the unit cell volume decreases [79], and the tilting angle (Fig. 5d) increases [80]. The τ_ε is also related to the tolerance factor [74], as shown in Fig. 5b.

It is possible for the "Glazer-like" tilting in the compounds to affect the dielectric properties. Thus, the selection for the composition x and the rare earth element R of the tungsten bronze type ceramic $Ba_{6-3x}R_{8+2x}Ti_{18}O_{54}$ are: (as concluded in Ref. [80]) 1) for high *Q·f*, the composition x should be 2/3; 2) for high ε_r, certain R ions should be selected with large polarizability and appropriate radius to gain large octahedral volume and small tilting angle.

Conductivity

The oxygen octahedral tilting can reduce the overlap between the B d and O 2p orbitals and hence affects the electric bandgap of the perovskite oxides. As we mentioned before, BFO is an insulating ferroelectric, and its conductivity is highly related to the tilting. As illustrated in Fig. 6a, at the ferroelectric domain walls of the BFO thin films, the local symmetry is damaged accompanied by the suppression of ferroelectric polarization, leading to a lattice expansion in the direction perpendicular to the domain walls. Therefore, the octahedral tilting is suppressed, giving rise to straightening of the Fe–O–Fe bond angle and increasing of the overlap between Fe and O orbitals and hence conductive domain walls. Consequently, the domain-wall conductivity also depends on the type of domain wall. For example, if the absolute value of the polarizations at the domain walls are low, the volume change will be greater, making the domain walls more conductive. In rhombohedral BFO, there are three types of domain walls: 180°, 109° and 71°, as defined by the polarizations direction in the adjacent domains across the wall. The tilting is not suppressed in 180° domain wall, hence, the absolute polarization is zero. Thus, this type of domain wall is more conductive. The tilting is the most suppressed in the 71° wall, and therefore it has the biggest polarization value, and the least conductivity. The experimental observations of domain wall conductivities agree with this prediction [81,82]. First principle calculation studies [83,84] further explained that the oxygen octahedral tilting related distortions play the primary role in the ferroelectric phase, and thus control the domain wall

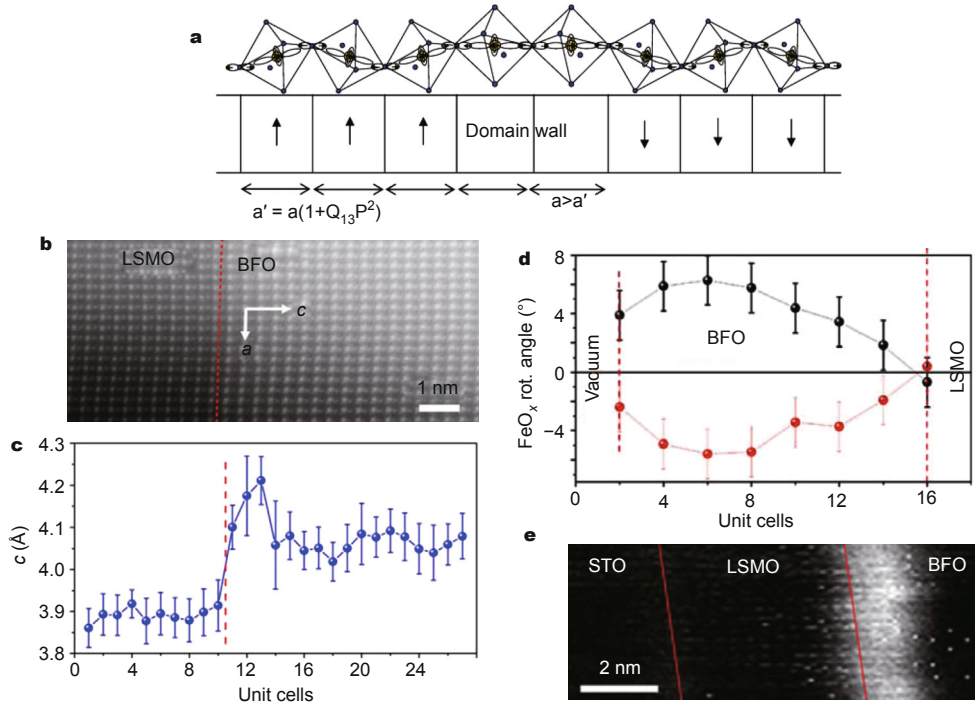

Figure 6 (a) Schematic of the polarization (arrows) and the oxygen octahedral tilting mode near an 180° domain wall in BFO (Reprinted with permission from Ref. [82], Copyright 2009, John Wiley and Sons). (b–e) Observation of the octahedral tilting at the epitaxial interface of BFO/LSMO/STO heterostructure. (b) The HAADF image of the BFO/LMSO interface. The Line profile of *c* parameter (c) and oxygen octahedral tilting angle (d) across the interface. (e) χ^2 map of low-loss EELS spectra imaging exhibits an anomaly response (Reprinted with permission from Ref. [85], Copyright 2010, American Physical Society).

conduction.

This lattice expansion induced conductivity change can be utilized through strain engineering during thin film growth. It was reported that the interface of the BFO/LSMO/STO structure has an anomaly electrical performance [85]. As shown in Figs 6b–d, the epitaxial thin LSMO layer passes on the strain to the first several unit cells of the BFO film adjacent to the interface. Using HAADF TEM (Fig. 6b), the *c* lattice parameter of the first 3-4 atomic layers of BFO has an increase from 4.06 Å to 4.21Å (Fig. 6c). The extension of the structure leads to a suppression of the oxygen octahedral tilting, and the FeO_x angles increase gradually in the BFO phase in the same region that shows the expanded *c*-lattice parameter (Fig. 6d). The higher symmetry at the interface is expected to influence the conductivity of the interface of BFO/LSMO similar to the conducting domain walls. The electronic behavior is measured by low-loss electron energy loss spectroscopy (EELS) imaging (Fig. 6e), that the decreasing of the bandgap at the interface comes mainly from an increase of the Fe–O–Fe angle to 180°, and therefore enhances the bandwidth. These results demonstrate a mesoscopic antiferrodistortive phase transition near the interface in BFO. By controlling the epitaxial strain from certain substrates, the oxygen octahedral tilting can be controlled to establish new phase and novel properties in oxide ABO_3 thin films, which proposes a new concept of the tilting-controlled phenomena.

CONCULSION AND FUTURE PERSPECTIVES

The oxygen octahedral tilting in ABO_3 perovskite structure is highly related to the physical properties. The tilting systems can affect the properties in two aspects: 1) triggering new properties by regulating the electron or/and spin degrees of freedom; 2) tuning the original properties to an unexpected level. Since the discovery of Glazer, the possible tilting structure for basic perovskite has been studied and narrowed down from 23 possible tilting systems as Glazer first claimed. However, researchers' interest of prediction for new structures never stopped. With the rapid development of thin film growth technics and structure detection measurements, new superstructures with complex tilting systems have been exploited. Furthermore, controllable strain from substrate or elaborate interface, as well as the traditional doping method in ceramics, have been utilized to alter the lattice symmetry at atomic level, and then create new performances. With regard to magnetic and electrical behaviors, the controlling of the oxygen octahedral titling can bring out novel influences on the spin/orbit distribution, the (spontaneous) polarization, and the energy band structure. By manipulating the tilting in perovskite or related structures, tunable magnetic and electrical properties can be used for device applications.

Received 23 March 2015; accepted 13 April 2015; published online 20 April 2015

1 Galasso FS. Structure, Properties, and Preparation of Perovskite-Type Compounds. London: Pergamon Press, 1969
2 Howard CJ, Stokes HT. Group theoretical analysis of octahedral tilting in perovskites. Acta Cryst B, 1998, 54: 782–789
3 Tidrow C. Mapping comparison of Goldschmidt's tolerance factor with perovskite structural conditions. Ferroelectrics, 2014, 470: 13–27
4 Millis AJ, Shraiman BI, Mueller R. Dynamic Jahn-Teller effect and colossal magnetoresistance in $La_{1-x}Sr_xMnO_3$. Phys Rev Lett, 1996, 77: 175–178
5 Pauling L. The Nature of the Chemical Bond (3rd Ed.). Ithaca: Cornell University Press, 1960
6 Wainer E, Soloman S. Titanium Alloy Manufacturing Co. Report 8–9, 1942
7 Corker DL, Glazer AM, Whatmore RW. A neutron diffraction investigation into the rhombohedral phases of the perovskite series $PbZr_{1-x}Ti_xO_3$. J Phys Condens Mat, 1998, 10: 6251–6269
8 Glazer AM, The classification of tilted octahedral in perovskites. Acta Cryst B, 1972, 28: 3384–3392
9 He J, Borisevich A, Kalinin SV, *et al*. Control of octahedral tilts and magnetic properties of perovskite oxide heterostructures by substrate symmetry. Phys Rev Lett, 2010, 105: 227203
10 Bousquet E, Dawber M, Stucki N, *et al*. Improper ferroelectricity in perovskite oxide artificial superlattices. Nature, 2008, 452: 732–736
11 Von Hippel AR. Molecular Science and Molecular Engineering. Cambridge: MIT Press, 1959
12 Megaw H. Crystal structure of barium titanate. Nature, 1945, 155: 484–485
13 Bhalla AS, Guo R, Roy R. The perovskite structure—a review of its role in ceramic science and technology. Mat Res Innovat, 2000, 4: 3–26
14 Reaney I, Colla E, Setter N. Dielectric and structural characteristics of Ba-based and Sr-based complex perovskites as a function of tolerance factor. Jpn J Appl Phys 1, 1994, 33: 3984–3990
15 Eng HW, Barnes PW, Auer BM, *et al*. Investigations of the electronic structure of d(0) transition metal oxides belonging to the perovskite family. J Solid State Chem, 2003, 175: 94–109
16 Wang Y, Sui Y, Ren P, *et al*. Correlation between the structural distortions and thermoelectric characteristics in $La_{1-x}A_xCoO_3$ (A = Ca and Sr). Inorg Chem, 2010, 49: 3216–3223
17 Pei S, Jorgensen JD, Dabrowski B, *et al*. Structural phase diagram of the $Ba_{1-x}K_xBiO_3$ system. Phys Rev B, 1990, 41: 4126–4141
18 Perillat-Merceroz C, Gauthier G, Roussel P. Synthesis and study of a Ce-doped La/Sr titanate for solid oxide fuel cell anode operating directly on methane. Chem Mater, 2011, 23: 1539–1550
19 Jin KX, Chen CL, Wang SL, *et al*. Photoresponsive character of double-doped $La_{2/3}(Ca_{1/3}Sr_{2/3})_{1/3}MnO_3$ film. J Appl Phys, 2004, 96: 1537–1539
20 Goodenough JB. Theory of the role of covalence in the perovskite-type manganites [La, M(II)]MnO_3. Phys Rev, 1955, 100: 564–573
21 Kanamori J. Crystal distortion in magnetic compounds. J Appl Phys, 1960, 31: S14–S23
22 Ramesh R, Spaldin NA. Multiferroics: progress and prospects in thin films. Nat mater, 2007, 6: 1476–1122
23 Nan CW, Bichurin MI, Dong S, Viehland D, Srinivasan G. Multiferroic magnetoelectric composites: historical perspective, status, and future directions. J Appl Phys, 2008, 103: 031101
24 Glazer AM. Simple ways of determining pervoskite structures. Acta cryst A, 1975 31: 756–762
25 Goldschmidt VM. The laws of crystal chemistry. Naturwissenschaften, 1926, 14: 477–485

26 Wells AF. Structural Inorganic Chemistry. London: Oxford Science publications, 1995
27 Müller U. Inorganic Structural Chemistry. Chichester: Wiley & Sons Ltd, 1993
28 Galasso FS, Katz L. Preparation and structure of $Ba_5Ta_4O_{15}$ and related compounds. Acta Cryst, 1961, 14: 647
29 Goodenough JB. Electronic and ionic transport properties and other physical aspects of perovskites. Rep Prog Phys, 2004, 67: 1915–1993
30 Rondinelli JM, Spaldin NA. Structure and properties of functional oxide thin films: insights from electronic-structure calculations. Adv Mater, 2011, 23: 3363–3381
31 Rondinelli JM, Coh S. Large isosymmetric reorientation of oxygen octahedra rotation axes in epitaxially strained perovskites. Phys Rev Lett, 2011, 106: 235502
32 Wang D, Salje EKH, Mi SB, Jia CL, Bellaiche L. Multidomains made of different structural phases in multiferroic $BiFeO_3$: a first-principles-based study. Phys Rev B, 2013, 88: 134107
33 Prosandeev S, Wang D, Ren W, *et al*. Novel nanoscale twinned phases in perovskite oxides. Adv Funct Mater, 2013, 23: 234–240
34 Mitchell JF, Argyriou, DN, Potter CD, *et al*. Structural phase diagram of $La_{1-x}Sr_xMnO_{3+\delta}$: relationship to magnetic and transport properties. Phys Rev B, 1996, 54: 6172–6183
35 Kennedy BJ, Howard CJ, Chakoumakos BC. Phase transitions in perovskite at elevated temperatures—a powder neutron diffraction study. J Phys Condens Mat, 1999, 11: 1479–1488
36 Dabrowski B, Avdeev M, Chmaissem O, *et al*. Freezing of octahedral tilts below the Curie temperature in $SrRu_{1-v}O_3$ perovskites. Phys Rev B, 2005, 71: 104411
37 Aso R, Kan D, Shimakawa Y, Kurata H. Atomic level observation of octahedral distortions at the perovskite oxide heterointerface. Sci Rep, 2013, 3: 2214
38 Iliev MN, Abrashev MV, Lee HG, *et al*. Raman spectroscopy of orthorhombic perovskitelike $YMnO_3$ and $LaMnO_3$. Phys Rev B, 1998, 57: 2872–2877
39 Bielecki J, Svedlindh P, Tibebu DT, *et al*. Structural and magnetic properties of isovalently substituted multiferroic $BiFeO_3$: insights from Raman spectroscopy. Phys Rev B, 2012, 86: 184422
40 Xu Q, Zheng X, Wen Z, *et al*. Enhanced room temperature ferromagnetism in porous $BiFeO_3$ prepared using cotton templates. Solid State Commun, 2011, 151: 624–627
41 Kiselev SV, Kshnyakina AN, Ozerov RP, *et al*. A neutron-diffraction study of the magnetic ordering and atomic displacements in some iron-containing perovskite substances with special dielectric properties. Fizika Tverdogo Tela, 1963, 5: 3312–3316
42 Teague JR, Gerson R, James WJ. Dielectric hysteresis in single crystal $BiFeO_3$. Solid State Commun. 1970, 8: 1073
43 Moreau JM, Michel C, Gerson R, *et al*. Ferroelectric $BiFeO_3$ X-ray and neutron diffraction study. J Phys Chem Solids, 1971, 32: 1315–1320
44 Filip'ev VS, Smol'yaninov IP, Fesenko EG, *et al*. Synthesis of $BiFeO_3$ and determination of the unit cell. Kristallografiâ, 1960, 5: 913–914
45 Kubel F, Schmid H. Structure of a ferroelectric and ferroelastic monodomain crystal of the perovskite $BiFeO_3$. Acta Cryst B, 1990, 46: 698–702
46 Shannon RD. Revised effective ionic radii and systematic studies of interatomic distances in halides and chalcogenides. Acta Cryst A, 1976, 32: 751–767
47 Palewicz A, Przeniosło R, Sosnowska I, Hewat AW. Atomic displacements in $BiFeO_3$ as a function of temperature: neutron diffraction study. Acta Cryst A, 2007, 63: 537–544
48 Megaw HD, Darlington CNW. Geometrical and structural relations in rhombohedral perovskites. Acta Cryst A, 1975, 31: 161–173
49 Ederer C, Spaldin NA. Weak ferromagnetism and magnetoelectric coupling in bismuth ferrite. Phys Rev B, 2005, 71: 060401
50 Lebeugle D, Colson D, Forget A, *et al*. Electric-field-induced spin flop in $BiFeO_3$ single crystals at room temperature. Phys Rev Lett, 2008, 100: 227602
51 Wang N, Cheng J, Pyatakov A, *et al*. Multiferroic properties of modified $BiFeO_3$-$PbTiO_3$-based ceramics: random-field induced release of latent magnetization and polarization. Phys Rev B, 2005, 72: 104434
52 Bai F, Wang J, Wuttig M, *et al*. Destruction of spin cycloid in (111)(c)-oriented $BiFeO_3$ thin films by epitiaxial constraint: enhanced polarization and release of latent magnetization. Appl Phys Lett, 2005, 86: 032511
53 Dzyaloshinskii IE. A thermodynamic theory of "weak" ferromagnetism of antiferromagnetics. J Phys Chem Solids, 1958, 4: 241–255
54 Moriya T. Anisotropic superexchange interaction and weak ferromagnetism. Phys Rev, 1960, 120: 91–98
55 Shvartsman VV, Kleemann W, Haumont R, Kreisel J. Large bulk polarization and regular domain structure in ceramic $BiFeO_3$. Appl Phys Lett, 2007, 90: 172115
56 Wang JJ, Hu JM, Yang TN, *et al*. Effect of strain on voltage-controlled magnetism in $BiFeO_3$-based heterostructures. Sci Rep, 2014, 4, 4453
57 Heron JT, Bosse JL, He Q, *et al*. Deterministic switching of ferromagnetism at room temperature using an electric field. Nature, 2014, 516: 370–373
58 Zeches RJ, Rossell MD, Zhang JX, *et al*. A strain-driven morphotropic phase boundary in $BiFeO_3$. Science, 2009, 326: 977–980
59 He Q, Chu YH, Heron JT, *et al*. Electrically controllable spontaneous magnetism in nanoscale mixed phase multiferroics. Nat Commun, 2011, 2: 225
60 Asamitsu A, Moritomo Y, Tomioka Y, *et al*. A structural phase-transition induced by an external magnetic-field. Nature, 1995, 373: 407–409
61 Gong GQ, Canedy C, Xiao G, *et al*. Colossal magnetoresistance of 1,000,000-fold magnitude achieved in the antiferromagnetic phase of $La_{1-x}Ca_xMnO_3$. Appl Phys Lett, 1995, 67: 1783–1785
62 Caignaert V, Maignan A, Raveau B. Up to 50,000 percent resistance variation in magnetoresistive polycrystalline perovskites $Ln_{2/3}Sr_{1/3}MnO_3$ (Ln = Nd; Sm). Solid State Commun, 1995, 95: 357–359
63 Van Roosmalen JAM, Cordfunke EHP, Helmholdt RB, *et al*. The defect chemistry of $LaMnO_{3\pm\delta}$: 2. structural aspects of $LaMnO_{3+\delta}$. J Solid State Chem, 1994, 110: 100–105
64 Millis AJ, Littlewood PB, Shraiman BI. Double exchange alone does not explain the resistivity of $La_{1-x}Sr_xMnO_3$. Phys Rev Lett, 1995, 74: 5144–5147
65 Fujishiro H, Fukase T, Ikebe M. Charge ordering and sound velocity anomaly in $La_{1-x}Sr_xMnO_3$ ($x \geq 0.5$). J Phys Soc Japan, 1998, 67: 2582–2585
66 Cesaria M, Caricato AP, Maruccio G, Martino M. LSMO-growing opportunities by PLD and applications in spintronics. J Phys Conf Ser, 2011, 292: 012003
67 Dabrowski B, Avdeev M, Chmaissem O, *et al*. Freezing of octahedral tilts below the Curie temperature in $SrRu_{1-v}O_3$ perovskites. Phys Rev B, 2005, 71: 104411
68 Dagotto A, Hotta T, Moreo A. Colossal magnetoresistant materials: the key role of phase separation. Phys Rep, 2001, 344: 1–153
69 Park JH, Vescovo E, Kim HJ, *et al*. Direct evidence for a half-metallic ferromagnet. Nature, 1998, 392: 794–796
70 Cockayne E, Burton BP. Phonons and static dielectric constant in $CaTiO_3$ from first principles. Phys Rev B, 2000, 62: 3735–3743
71 Miyake S, Ueda R. On polymorphic change of $BaTiO_3$. J Phys Soc Jpn, 1946, 1: 32–33
72 Cohen RE. Origin of ferroelectricity in pervoskite oxides. Nature, 1992, 6382: 136–138
73 Colla EL, Reaney IM, Setter N. Effect of structural changes in complex perovskites on the temperature coefficient of the relative per-

mittivity. J Appl Phys, 1993, 74: 3414–3425
74 Reaney IM, Ubic R. Dielectric and structural characteristics of perovskites and related materials as a function of tolerance factor. Ferroelectrics, 1999, 228: 23–38
75 Kolar D, Stadler Z, Gaberscek S, Suvorov D. Ceramic and dielectric properties of selected compositions in the BaO-TiO_2-Nd_2O_3 system. Ber Dt Keram Ges, 1978, 55: 346–347
76 Ohsato H, Ohhashi T, Kato H, *et al.* Microwave dielectric-properties and structure of the $Ba_{6-3x}Sm_{8+2x}Ti_{18}O_{54}$ solid solution. Jpn J Appl Phys 1, 1993, 34: 187–191
77 Fukuda K, Kitoh R, Awai I. Microwave characteristics of mixed phases of $BaPr_2Ti_4O_{12}$-$BaPr_2Ti_5O_{14}$ ceramics. J Mater Res, 1995, 10: 312–319
78 Ohsato H, Mizuta M, Ikoma T, *et al.* Microwave dielectric properties of tungsten bronze type $Ba_{6-3x}R_{8+2x}Ti_{18}O_{54}$ (R = La, Pr, Nd and Sm) solid solutions. J Ceram Soc Japan, 1998, 106: 178–182
79 Valant M, Suvorov D, Rawn CJ. Intrinsic reasons for variations in dielectric properties of $Ba_{6-3x}R_{8+2x}Ti_{18}O_{54}$ (R = La-Gd) solid solutions. Jpn J Appl Phys 1, 1999, 38: 2820–2826
80 Ohsato H. Science of tungstenbronze-type like $Ba_{6-3x}R_{8+2x}Ti_{18}O_{54}$ (R = rare earth) microwave dielectric solid solutions. J Eur Ceram Soc, 2001, 21: 2703–2711
81 Seidel J, Martin LM, He Q, *et al.* Conduction at domain walls in oxide multiferroics. Nat Mater, 2009, 8: 229–234
82 Catalan G, Scott JF. Physics and application of bismuth ferrite. Adv Mater, 2009, 21: 2463–2485
83 Daumont CJM, Farokhipoor S, Ferri A, *et al.* Tuning the atomic and domain structure of epitaxial films of multiferroic $BiFeO_3$. Phys Rev B, 2010, 81: 144115
84 Diéguez O, Aguado-Puente P, Junquera J, Íñiguez J. Domain walls in a perovskite oxide with two primary structural order parameters: first-principles study of $BiFeO_3$. Phys Rev B, 2013, 87: 024102
85 Borisevich AY, Chang HJ, Huijben M, *et al.* Suppression of octahedral tilts and associated changes in electronic properties at epitaxial oxide heterostructure interfaces. Phys Rev Lett, 2010, 105: 087204

Acknowledgment This work was supported by the National Natural Science Foundation of China (51272121, 51221291, and 51328203). We thank Fei Xu for discussions and the comments on the manuscript.

Author contributions Gao Y collected and categorized the literatures. Gao Y and Wang J wrote the manuscript. Wu L provided comments and feedback on the manuscript. Bao S edited the figures. Lin Y provided the overall concept. Lin Y and Nan C supervised the manuscript writing and provided advice. All authors contributed to the general discussion.

Conflict of interest The authors declare that they have no conflicts of interest.

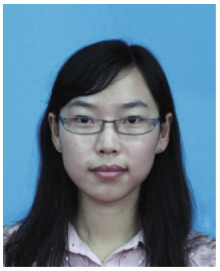

Ya Gao received her BSc degree from the School of Materials Science and Engineering, Tsinghua University in 2011. And then she joined Prof. Nan's group as a PhD candidate. Her research interests focus on multiferroic magnetoelectric materials and their applications in the field of memories and spintronic devices.

Yuanhua Lin is a "Changjiang Scholar" distinguished professor of Materials Science at the School of Materials Science and Engineering, Tsinghua University, Beijing, China. He received his BSc degree from East China Institute of Technology, MSc degree from the Chemical and Metallurgic Institute, Chinese Academy of Sciences, and PhD degree from Tsinghua University. He was a Japan Society for the Promotion of Science scholar at the University of Tokyo in 2005. His main research interests are functional oxide-based ceramics and thin films including high dielectric constant ceramics and thin films for high energy density capacitors applications, high-temperature oxide thermoelectric materials and devices for energy conversion.

Cewen Nan is a professor of Materials Science at the School of Materials Science and Engineering, Tsinghua University, Beijing, China. Before joining the faculty of Tsinghua University in 1999, he had worked in Wuhan University of Technology, Wuhan, China, since 1985. He was elected academician of Chinese Academy of Sciences in 2011 and the Third-World Academy of Sciences (TWAS) in 2012. His recent research focuses on functional materials, including multiferroic magnetoelectric materials, thermoelectric oxides, functional polymer-based composites, and solid state electrolytes.

中文摘要 钙钛矿结构氧化物具有极其多样化的物理性能, 如磁性、介电性、光电性、铁电性等. 钙钛矿晶胞中的氧离子排布成八面体结构. 氧八面体的变形或旋转会改变原有的物理特性, 甚至产生原本不存在的新性能. 本文综述了几种典型钙钛矿氧化物的氧八面体旋转与磁性能和电性能的关系, 同时探讨了如何通过样品制备控制微观的八面体旋转, 从而更有效的设计具有高性能的新结构, 及其潜在应用.